USRP-Based Indoor Channel Sounding for D2D and Multi-Hop Communications

Arvind Merwaday[1], Nadisanka Rupasinghe[1], İsmail Güvenç[1], Walid Saad[2], and Murat Yuksel[3]
[1]Electrical and Computer Engineering, Florida International University, Miami, FL 33174
[2]Electrical and Computer Engineering, University of Miami, Coral Gables, FL 33146
[3]Computer Science and Engineering, University of Nevada-Reno, Reno, NV 89557
Email: {amerw001, rrupa001, iguvenc}@fiu.edu, [2]walid@miami.edu, [3]yuksem@cse.unr.edu

***Abstract*—In wireless networks, mobile nodes with limited power budget must rely on multi-hop transmissions so as to achieve reliable communication with a distant peer device. Hence, it is of paramount importance to study the characteristics of wireless transmission over multi-hop links and its benefits over single-hop communication. In this work, a simulator is developed to assess the bit error rate (BER) performance of multi-hop, multi-carrier communication systems. The channel model used in the simulator is developed based on the channel statistics obtained through indoor channel measurements performed using the universal software radio peripherals (USRPs). As the bandwidth supported by a USRP device is much smaller than the channel bandwidth of interest, we use a frequency domain approach to measure the impulse response of wide band channel. By using the channel measurements, we show the impact of communication distance on the delay spread and coherence bandwidth of the channel. Our simulation results with orthogonal frequency division multiplexing (OFDM) systems show that the BER performance of multi-hop communication is better than the single-hop communication. The BER performance difference between the two cases becomes more significant for wider subcarrier frequency spacing.**

***Index Terms*—channel estimation, device-to-device, multi-hop, USRP.**

I. Introduction

Device-to-device (D2D) communication has recently received significant interest due to its potential benefits to achieve higher throughput and offer proximity based services [1], [2]. As a technology component of ongoing LTE Rel-12 standardization, it is also considered an important enabler for public safety communication as it can be deployed rapidly with or without fixed infrastructure [3]. In general, the devices of a D2D network are battery powered and have stringent transmit power requirements. Therefore, the devices can benefit from multi-hop communication with the peer devices acting as relay nodes. In such a multi-hop network, the devices can communicate with one another over a much larger geographical area.

This research was supported in part by the U.S. National Science Foundation under the grants CNS-1406968, CNS-1253731 and CNS-1406947.

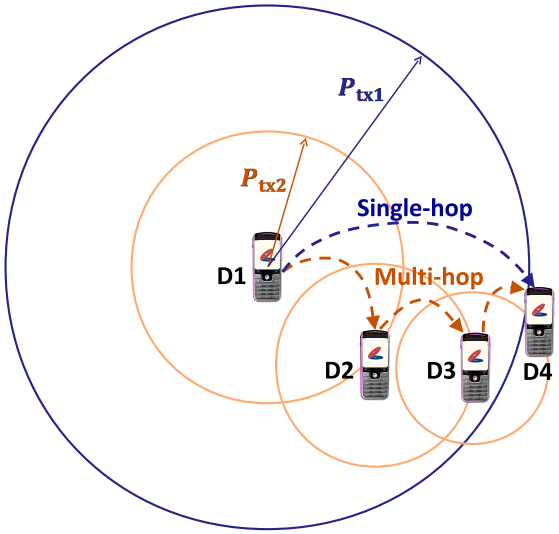

Fig. 1. Illustration of multi-hop communication.

Consider a D2D scenario as illustrated in Fig. 1 where the device D1 may communicate with D4 directly through single-hop transmission or through multi-hop transmission by using D2 and D3 as relay nodes. With transmit power control in the devices, the *signal to noise plus interference ratio* (SINR) at all the receivers are assumed to be constant. Then, the area of the large blue circle can be intuitively thought of as the power spent by D1 to communicate with D4. With this intuition, in the multi-hop case, the total area of the three small orange circles is smaller than the large blue circle. Thus, the total power spent in multi-hop case is smaller than that of the single-hop case. Moreover, larger coverage circle of D1 in single-hop case indicates higher interference caused to other devices. Therefore, multi-hop communication minimizes the interference while the devices can achieve longer distance communication.

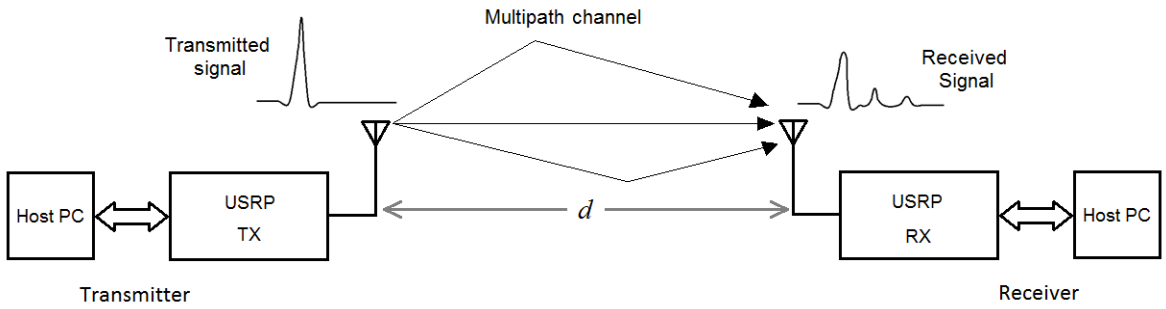

Fig. 2. System setup for channel measurements.

Today, a vast majority of wireless communication technologies such as WiFi and LTE, use *orthogonal frequency division multiplexing* (OFDM) in which the coherence bandwidth and Doppler spread of the channel are critical parameters. These parameters help in the dimensioning of the parameters of OFDM systems. Such parameters include the subcarrier frequency spacing, symbol duration, and cyclic prefix duration. In indoor channels, the Doppler effect can be considered negligible due to the low mobility of devices. To assess the performance of multi-hop communication in a D2D scenario, studying the channel impulse response (CIR) is important. Most of the channel measurement implementations in the literature make use of expensive equipment such as vector network analyzer, spectrum analyzer, and spread spectrum channel sounder as in [4] and [5]. On the other hand, the recently introduced *universal software radio peripheral* (USRP) platform provides an inexpensive solution to perform the channel measurements while providing a flexible solution due to its small form factor.

Channel sounders are implemented in [6]-[8] using USRPs with GNU Radio software platform. In [6] and [7], pseudo-random sequences are used for channel sounding. However, the temporal resolution of the estimated CIR is limited by the smaller bandwidth of USRP. In [8], a frequency domain channel estimator is implemented in which the carrier frequency is swept across a wide band channel to get a better temporal resolution of the estimated CIR.

The main contributions of this paper are: 1) to develop a frequency domain wide band channel estimation method using the USRP platform that supports smaller bandwidths (20 MHz) when compared to the channel bandwidth of interest, 2) to perform channel measurements with different distances between the transmitter and the receiver, and determine channel statistics such as path-loss, mean excess delay, root mean square (RMS) delay spread, and coherence bandwidth, 3) to build an empirical channel model as a function of distance by using the measured channel statistics, and 4) to incorporate the developed channel model into the multi-hop simulation model for evaluating the bit error rate (BER) performance of multi-carrier systems. In the multi-hop simulation model, two devices separated by a distance d communicate with each other in single-hop and two-hop scenarios. Using OFDM, the resulting average BERs with single and two-hop cases are compared for different distances and subcarrier frequency spacings.

II. Channel Sounding Method with USRPs

Two USRP devices from National Instruments [9] are used in the setup as shown in Fig. 2. Each USRP is controlled by a host PC and the transmitter and receiver operations are developed using Labview software. A transmitted signal is attenuated, delayed, phase shifted, and gets corrupted with noise as it travels through the channel. The signal received by the RX USRP exhibits fading effects due to multi-path propagation.

A. Channel Sounding Approach

Channel sounding is done by transmitting N narrow-band sinusoidal signals that are regularly spaced (Δf) in the frequency domain as illustrated in Fig. 3. Since the bandwidth of USRP is smaller than the channel bandwidth, the carrier frequency f_{ci} is swept across the channel bandwidth in N discrete steps, $i = 1, 2, .., N$. At each frequency step, a complex DC base-band signal frame consisting of 1000 samples is sent to the USRP. The USRP upconverts the DC signal to the carrier frequency f_{ci}.

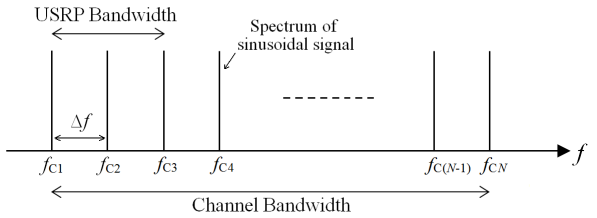

Fig. 3. Aggregated spectrum of all the sinusoidal signals.

The receiver initially sets the carrier frequency to f_{C1} and after receiving each frame, increments the carrier frequency by Δf. In this way, the carrier frequency sweep process at the receiver is synchronized with the transmitter. At each frequency step, beginning of the signal frame is identified via threshold detection of the received signal power. When a frame is detected and captured, it is downconverted to the base-band and

sent to the host PC. Carrier frequency offset and phase offset corrections are performed at the host PC to obtain the complex DC signal whose magnitude and phase represents the channel response at frequency f_{ci}.

B. Synchronization, Sweep Rate, and Calibration

At the receiver USRP, robust algorithms should be used to track the transmitter carrier frequency during the frequency sweep process as the transmitter and receiver USRPs use different timing references. We used power threshold detection method at the receiver's host computer to detect the signal. For longer distances between the transmitter and the receiver, dynamic range of the received power increases over the frequency band and the signal power may not be detected at some frequencies due to deep fades. In those cases, synchronization using the timing reference at the hardware level is reliable than using the host computer. Therefore, programming the FPGA in USRP to periodically change the carrier frequency can improve the sweep rate significantly. This method along with the power threshold detection of signal can improve the synchronization.

The transmitter power and receiver gain of the USRPs vary with the carrier frequency and are not calibrated. It is necessary to know these values to accurately estimate the amplitudes of received impulse response and for path-loss calculations. We used the *Mixed Domain Oscilloscope* to find the USRP transmit power and USRP receiver gain in the frequency band of interest.

C. Extracting Multipath Channel Parameters

After capturing all the frames in a sweep, the magnitude and phase values at all the frequencies are aggregated to form the frequency response of the channel. Then, computing the *inverse fast Fourier transform* (IFFT) will provide the CIR $h[n] = h(nT_{\rm s})$, where $T_{\rm s} = 1/(N\Delta f)$ is the sample period and n is the discrete time index. With K CIR measurements, the average *power delay profile* (PDP) can be obtained by, $\overline{PDP}[n] = \frac{1}{K}\sum_{k=1}^{K}|h_k[n]|^2$. The mean excess delay and RMS delay spread can be respectively evaluated as

$$\overline{\tau} = \frac{\sum\limits_{\forall n} n\ T_{\rm s}\ \overline{PDP}[n]}{\sum\limits_{\forall n}\overline{PDP}[n]}, \qquad \overline{\tau}_{\rm rms} = \sqrt{\overline{\tau^2} - (\overline{\tau})^2}, \quad (1)$$

where

$$\overline{\tau^2} = \frac{\sum\limits_{\forall n}(n\ T_{\rm s})^2\ \overline{PDP}[n]}{\sum\limits_{\forall n}\overline{PDP}[n]}. \quad (2)$$

Using the RMS delay spread, channel coherence bandwidth can be approximated as $B_{\rm c} \approx 1/(5\ \tau_{\rm rms})$ [10].

III. Channel Propagation Modeling

The impact of large scale propagation effects on the received signal are captured by *path loss (PL) and shadowing models*, while the small scale propagation effects are captured by *channel impulse response model*.

A. Path loss and shadowing models

We model the average PL at a distance d from the transmitter as,

$$\overline{PL}_{\rm dB}(d) = \overline{PL}_{\rm dB}(d_0) + \alpha\ 10\log_{10}(d/d_0), \quad (3)$$

where, α is the path-loss exponent and $\overline{PL}_{\rm dB}(d_0)$ is the PL at a reference distance $d_0 = 1$ m from the transmitter. Using the *curve fitting tool* in Matlab, we find the value of α that provides a best fit of (3) to the measured average PL values. The measured average PL values with respect to d_0 can be obtained using

$$\overline{PL}^{\rm meas}_{\rm dB}(d) = \overline{PL}^{\rm meas}_{\rm dB}(d_0) + 10\log_{10}\left(\frac{E_{\rm rx0}}{E_{\rm rx}(d)}\right), \quad (4)$$

where, $E_{\rm rx}(d)$ and $E_{\rm rx0}$ are the total energies received from all the multi path components (MPCs) at distances d and d_0, respectively. These energies can be determined using the measured PDPs as $E_{\rm rx}(d) = \sum_{\forall n}\overline{PDP}[n]$.

Shadow fading is modeled using a log-normally distributed variable with zero mean and standard deviation σ. We denote this variable in decibel scale as $X_\sigma \sim \mathcal{N}(0,\sigma)$. The σ is assumed to be independent of d and its value can be found by fitting the Gaussian PDF to the histogram of the measured samples.

B. Channel impulse response model

Theoretically, the CIR $h(t)$ is composed of an infinite number of MPC arrivals, which can be expressed by

$$h(\tau) = \sum_{i=1}^{\infty} a_i e^{j\phi_i}\delta(\tau - \tau_i), \quad (5)$$

where, τ_i denotes the delay of the ith arrival in propagation between the transmitter and the receiver. The a_i and $\phi_i \sim \mathcal{U}[0, 2\pi]$ [11] represent, respectively, the amplitude and phase shift of the ith arrival. It is possible to completely determine the PDP by a set of samples spaced by $\Delta\tau = 1/W$, where W is the bandwidth of the channel [12] (i.e., $\tau_k = k/W, k = 0, 1, 2, \ldots$). Each sample in the set is the power of all MPCs arrived during the delay bin $\Delta\tau$. Then, the PDP can be expressed as,

$$\tilde{p}(\tau) = \sum_{k=1}^{\infty}\tilde{p}_k\delta(\tau - \tau_k), \quad (6)$$

where, $\tilde{p}_k$ is the power contained in the kth bin. The total energy in the PDP of (6) is normalized such that

$\sum_{k=1}^{\infty} \tilde{p}_k = 1$. With this approach, p_k (in dB) for LOS case can be given as [13]

$$p_k = \begin{cases} C & k = 0, \\ Q + r - \beta \frac{\tau_k}{\overline{\tau}_{rms}} + s_k & k > 0, \end{cases} \quad (7)$$

where, Q is the normalizing factor that makes the sum of all $\tilde{p}_k$'s equals to unity, r is the difference between the power of second MPC and the power of first MPC which can be modeled as a Gaussian distribution with mean μ_r and variance σ_r, and β is the power decay coefficient of the MPCs in the PDP. The RMS delay spread $\overline{\tau}_{rms}$ is used as a normalizing factor, so that β is dimensionless. The variable s_k accounts for the random variations in PDP which can be modeled as a Gaussian distribution with zero mean and variance σ_s.

The random variable C is the power of the first MPC in PDP that can be modeled as

$$C = C_0 - \gamma_c \log_{10}(d) + \epsilon_c, \quad (8)$$

where, C_0 is the average power of the first MPC at the reference distance d_0, γ_c is a coefficient that accounts for the power decay of the first MPC with distance d, and ϵ_c is a zero mean Gaussian random variable with variance σ_c.

The power decay coefficient β in (7) is modeled as

$$\beta = \beta_0 - \gamma \log_{10}(d) + \epsilon, \quad (9)$$

where, β_0 is the average decay of PDP at the reference distance, γ is a coefficient that accounts for the power decay of first MPC with distance d, and ϵ is a zero mean Gaussian random variable with variance σ_ϵ.

IV. Measurement and Simulation Results

A. CIR Measurements

Using the channel sounding method described in Section II, CIR measurements of a 100 MHz channel were conducted in an indoor office environment for different *line of sight* (LOS) distances (10 m–27 m) between the transmitter and the receiver USRPs. For each distance, $K = 100$ CIR measurements were recorded. Fig. 4 shows the base-band equivalent CIR and frequency response measurements for a distance of 21 m. Fig. 5 shows the average PDP evaluated using the 100 CIR measurements at $d = 21$ m.

Using the measured CIRs, the calculated mean excess delay, RMS delay spread and coherence bandwidth of the channel are shown in Fig. 6 as a function of distance. It can be observed that the RMS delay of channel increases with increase in the distance, causing the coherence bandwidth to decrease significantly.

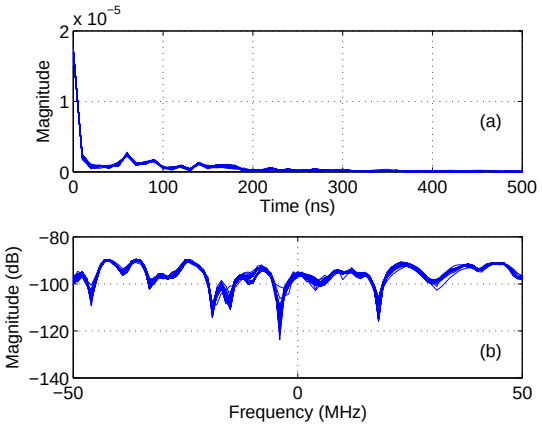

Fig. 4. Overlaid measurements of base-band equivalent (a) channel impulse responses; and (b) channel frequency responses; at a distance $d = 21$ m from the transmitter.

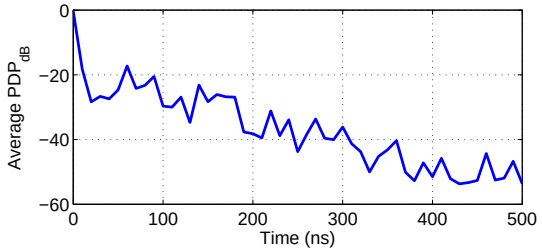

Fig. 5. Average PDP of the channel for $d = 21$ m.

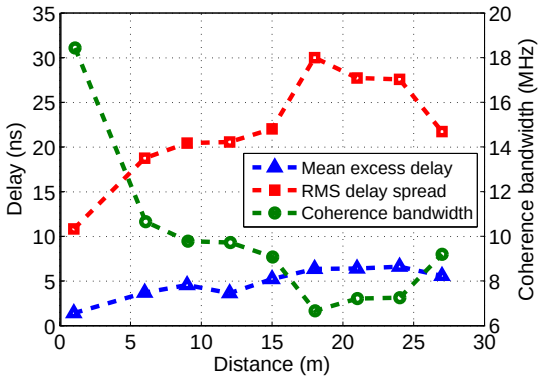

Fig. 6. Mean excess delay, RMS delay spread and coherence bandwidth of the channel.

B. Channel Modeling Parameters

Fig. 7 shows the measured average PL as a function of $10 \log_{10}(d)$ and the best line fit to the measured values. The best line fit was produced using (3) with $\alpha = 1.66$ and $\overline{PL}_{\text{dB}}(d_0) = 43.42$ dB. The α is observed to be less than the free-space path loss exponent $\alpha_{\text{FS}} = 2$. This could be due to walls of the corridor being close to each other that may cause strong reflections and refractions, as also reported in [14] for LOS scenarios.

The shadow fading model can be generated as described in Section III-A by finding the standard deviation of shadowing variable X_σ that best fits the Gaussian distribution to the histogram of the measured samples that include all distances and CIR measurements. Fig. 8

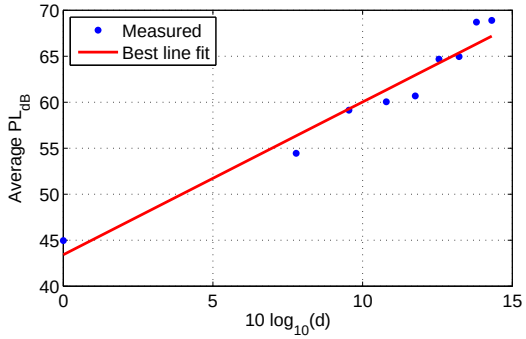

Fig. 7. Measured average path loss and the best line fit for different distances.

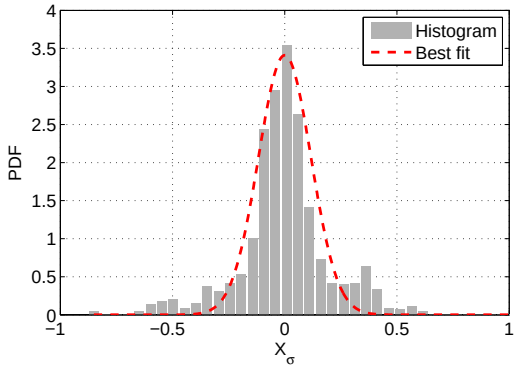

Fig. 8. Histogram of the shadowing variable X_σ and the best fitting Gaussian distribution.

shows the histogram and the best fitting Gaussian distribution with $\sigma = 0.117$ dB. This value of σ is close to the value obtained in [15] for an indoor scenario with a LOS link between the transmitter and the receiver.

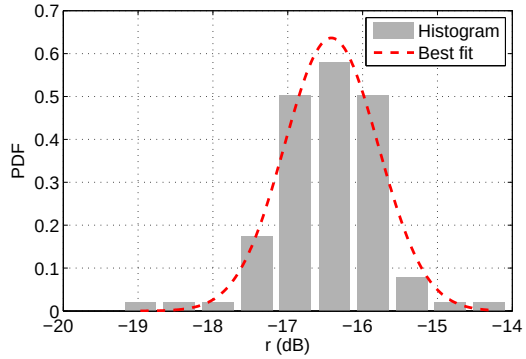

Fig. 9. Histogram of r and the best fitting Gaussian distribution.

Combining the path loss and shadowing models, the large scale fading can be expressed as,

$$PL_{\rm dB}(d) = \overline{PL}_{\rm dB}(d_0) + 16.6\log_{10}(d/d_0) + X_\sigma. \tag{10}$$

With reference to (7), the histogram of r which represents the difference between the power of second MPC and the power of first MPC is shown in Fig. 9. The best fitting Gaussian distribution is with the mean $\mu_r = -16.47$ dB and standard distribution $\sigma_r = 0.38$ dB. For s_k in (7), the histogram and the best fitting Gaussian distribution with $\sigma_s = 29.48$ dB are shown in Fig. 10. Similarly, other parameters of the channel model are found through regressions using (8) and (9), and Table I shows the extracted values of all the parameters. Using these parameters, our channel model is validated in Fig. 11, where the simulated PDP samples are compared with the measured PDP samples for different distances.

TABLE I
PARAMETERS OF CHANNEL MODEL

Parameter	Value
α	1.66
σ	0.12 dB
$\overline{PL}_{\rm dB}(d_0)$	43.42 dB
C_0	-56.62 dB
γ_c	21.91
σ_c	0.026
β_0	-0.64
γ	0.90
σ_ϵ	0.0052
σ_s	29.48 dB
μ_r	-16.47 dB
σ_r	0.38 dB

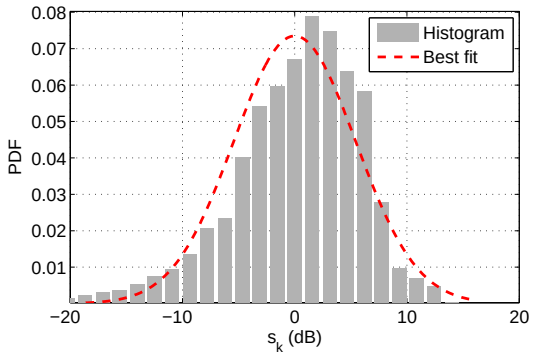

Fig. 10. Histogram of s_k and the best fitting Gaussian distribution.

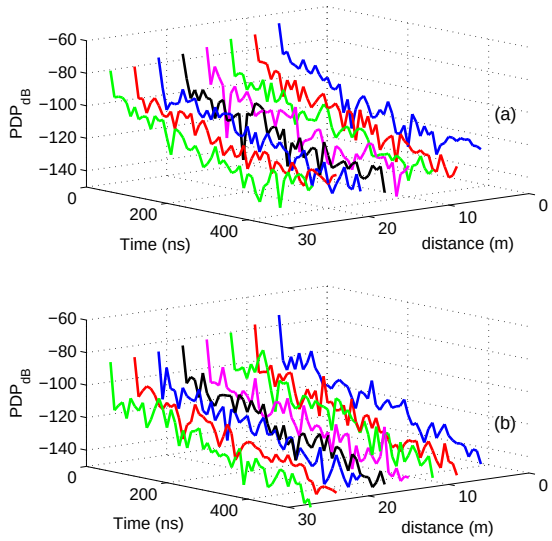

Fig. 11. Comparison of the (a) measured, and (b) simulated PDP samples for different distances.

C. Multi-hop versus Single-hop Performance

The simulation setup for multi-hop communication is illustrated in Fig. 12. Devices in the simulation use OFDM to communicate over the channel modeled in this paper, with the model parameters as summarized in Table I. The transmitter can communicate with the receiver over a relay node with two-hops, or directly with a single-hop by transmitting with higher transmission power. By using transmit power control, the received powers at the relay and receiver nodes are assumed to be identical for both single-hop and two-hop cases. On the other hand, the channel selectivity characteristics of single and two-hop scenarios will be different due to different communication distances. Our goal is to investigate the system-level impact of the channel selectivity characteristics on single-hop and multi-hop communications.

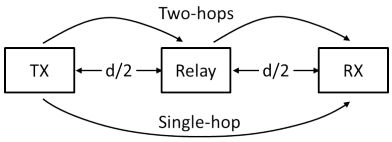

Fig. 12. Multi-hop communication.

Simulations are carried out for three different distances $(50, 75, 100$ m) between the TX and RX in Fig. 12, each with three different subcarrier frequency spacings $(60, 80, 100$ kHz). The number of subcarriers is fixed to 64, fifty two of which are the active subcarriers. With this simulation setup, we try to analyze how the distance and the OFDM subcarrier spacing affect the performance of multi-hop and single-hop communications.

The results that capture the detrimental effects of higher frequency selectivity in an OFDM system for the TX-RX link are shown in Fig. 13. From this figure, we can clearly see that multi-hop communication yields a lower BER for a channel with lower frequency selectivity. Accordingly, the BER difference between the single-hop and two-hop cases increases with increasing subcarrier frequency spacing. Nonetheless, Fig. 13 shows that multi-hop communication reduces the BER for all frequency spacing.

V. Concluding Remarks and Discussion

In this paper, we have performed channel impulse response measurements in an indoor office environment by using USRPs. A frequency domain channel sounding method is employed to characterize a wide-band channel of bandwidth greater than the USRP supported bandwidth. The channel measurement data is utilized to determine the large-scale and small-scale statistics of the channel, using which, a channel model is developed. Using this channel model in a multi-hop D2D simulator, we have analyzed the BER performance of single-hop and two-hop communication scenarios with respect to the distance between the source and destination nodes. Our simulation results show that the two-hop case provides significant improvement in the BER performance when compared to the single-hop case.

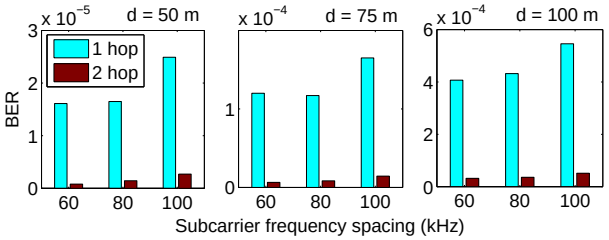

Fig. 13. BER for different distances and subcarrier frequency spacings.

References

[1] 3GPP, "Feasibility study on LTE device to device proximity services - radio aspects," Tech. Rep. (3GPP TR 36.843), 2013.

[2] A. Asadi, Q. Wang, and V. Mancuso, "A survey on device-to-device communication in cellular networks," *CoRR*, vol. abs/1310.0720, 2013.

[3] Qualcomm, Inc., "Study on LTE device to device proximity services," 3GPP Work Item Description (RP-122009), Spain, Dec. 2012.

[4] C. Holloway, W. Young, G. Koepke, K. Remley, D. Camell, and Y. Becquet, "Attenuation of radio wave signals coupled into twelve large building structures," Natl. Inst. Stand. Technol. Note 1545, Apr. 2008. [Online]. Available: http://www.eeel.nist.gov/kate papers/R12 TN1545.pdf

[5] D. Matolak, Q. Zhang, and Q. Wu, "Path loss in an urban peer-to-peer channel for six public-safety frequency bands," *IEEE Wireless Commun. Lett.*, vol. 2, no. 3, pp. 263–266, June 2013.

[6] A. L. Naour, O. Goubet, C. Moy, and P. Leray, "Spread spectrum channel sounder implementation with USRP platforms," SUPELEC engineering school. [Online]. Available: http://www.rennes.supelec.fr/ren/perso/cmoy/papers/Supelec_SDR11final.pdf

[7] D. Maas, M. Firooz, J. Zhang, N. Patwari, and S. Kasera, "Channel sounding for the masses: Low complexity GNU 802.11b channel impulse response estimation," *IEEE Trans. Wireless Commun.*, vol. 11, no. 1, pp. 1–8, Jan. 2012.

[8] M. N. Islam, B.-J. J. Kim, P. S. Henry, and E. Rozner, "A wireless channel sounding system for rapid propagation measurements," *CoRR*, vol. abs/1211.4940, 2012.

[9] National Instruments. (2014, Feb. 14) *NI USRP*. [Online]. Available: https://www.ni.com/usrp/

[10] R. W. Heath, "Introduction to wireless digital communication: A signal processing perspective," .

[11] C. Gentile, N. Golmie, K. Remley, C. Holloway, and W. Young, "A channel propagation model for the 700 MHz band," in *Proc. IEEE Int. Conf. Commun. (ICC)*, Cape Town, South Africa, May 2010, pp. 1–6.

[12] L. Greenstein, S. Ghassemzadeh, S.-C. Hong, and V. Tarokh, "Comparison study of UWB indoor channel models," *IEEE Trans. Wireless Commun.*, vol. 6, no. 1, pp. 128–135, Jan. 2007.

[13] S. Ghassemzadeh, L. Greenstein, T. Sveinsson, A. Kavcic, and V. Tarokh, "UWB delay profile models for residential and commercial indoor environments," *IEEE Trans. Veh. Technol.*, vol. 54, no. 4, pp. 1235–1244, July 2005.

[14] N. Udar, K. Kant, R. Viswanathan, and D. Cheung, "Ultra wideband channel characterization and ranging in data centers," in *Proc. IEEE Int. Conf. Ultra-Wideband (ICUWB)*, Singapore, Sep. 2007, pp. 322–327.

[15] A. Alvarez, G. Valera, M. Lobeira, R. Torres, and J. Garcia, "New channel impulse response model for UWB indoor system simulations," in *Proc. IEEE Veh. Technol. Conf. (VTC)*, vol. 1, Apr. 2003, pp. 1–5 vol.1.